# Complete Colloidal Synthesis of Cu_2SnSe_3 Nanocrystals with Crystal Phase and Shape Control

Jian-jun Wang, Pai Liu, Colin C. Seaton, and Kevin M Ryan*

Materials and Surface Science Institute (MSSI) and Department of Chemical and Environmental Sciences, University of Limerick, Limerick, Ireland

S *Supporting Information*

ABSTRACT: Here we report an investigation of systematic control of crystal phase in the ternary nanocrystal system, dicopper tin triselenide. Optimizing the synthetic parameters allows modulation between nucleation and growth in either the hexagonal or cubic phase. In addition to size controlled single crystals, the particles can be tuned to occur as 1D linear heterostructures or 3D tetrapods with growth in one phase and termination in the alternate.
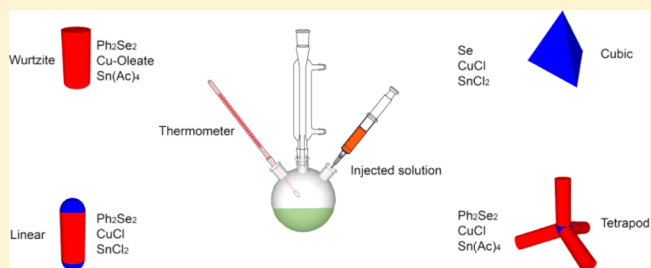
INTRODUCTION

Colloidal semiconductor nanocrystal syntheses represent a remarkable system where a relatively facile synthese masks a complex solution chemistry that can be modified to effect structural (size, morphology, and crystal phase) and physical properties (absorption, emission, conductivity) of the resultant particles.[1−7] The progress to this level of control has led to successful exploitation for multiple applications in electronics, solar energy conversion, thermoelectrics, and biomedicine.[7−14] In single crystal materials, the possible shapes attainable are determined by the allowed growth directions of the underlying crystal phase.[2,15,16] While preferential growth can be optimized through careful ligand selection that passivates certain facets allowing others to dominate, more complex three-dimensional (3D) shapes such as tetrapods are possible when the crystal nucleates in one phase followed by a growth in a different phase.[2,15−17]

Recently, Cu-based ternary ($I_2II−VI_3$) or quaternary ($I_2−II−IV−VI_4$) nanocrystals are attracting interest due to compositionally tunable band gaps, low toxicity, and ability to achieve high absorption coefficients using only earth abundant elements.[18−35] The colloidal synthesis, while utilizing a similar hot injection strategy to II−VI, is further complicated by the additional metal cations each having different chemical potentials with their availability as monomer to the growing crystals dictated by the decomposition kinetics of the respective precursors. A range of successful protocols to $CuInS_2$ (CIS), $CuIn_xGa_{1−x}S_2$ (CIGS), Cu_2ZnSnS_4 (CZTS), etc. have emerged around the goals of good crystal size control at the nanoscale utilizing a wide variety of precursors and reaction parameters.[29,30,36−43]

More recently the co-occurrence of two crystal phases in a single structure has allowed even greater shape evolution. Cabot and Yu, respectively, showed spherical (0D) and linear (1D) heterostructured morphologies arising from nucleation and growth in one phase before terminating in a different phase.[44,45] Recently we demonstrated the formation of (3D) Cu_2SnSe_3 tetrapods that nucleate with a cubic core with secondary growth of four wurtzite arms defining the tetrahedral geometry.[46] Many branching mechanisms have been demonstrated including polymorphism, twinning, oriented attachement, and crystal splitting.[47−49] More recently, branched ploypod $Cu_2Cd_xSnSe_y$ nanocrystals have also been obtained growing from tetrahedral (zinc-blende-like) to wurtzite with the assistance of a twinning mechanism.[49] The synthetic challenges surmounted to achieve each reported composition and structure have resulted in disparate protocols in terms of reagent choice, injection and growth temperatures, and growth times. As such, a systematic understanding of key influential factors toward complete phase and dimensional control in a single system has not been demonstrated.

Here we focus on the Cu_2SnSe_3 system that is interesting from the nanocrystal synthesis perspective as it crystallizes in either a stable cubic or wurtzite phase with relatively low-energy differentials. We show how fine-tuning the reaction chemistry can allow exquisite control of crystal phase and hence shape allowing homogeneous distributions of primary particles in either cubic or wurtzite form with subsequent progression to tetrapods (cubic core-wurtzite arms) or linear heterostructured nanocrystals (wurtzite core terminated by cubic ends). The interplay between subtle but critical temperature changes and choice of precursor is extrapolated to rationalize the morphology and shape changes observed.

EXPERIMENTAL SECTION

Materials. $CuCl_2\cdot 2H_2O$, CuCl, $SnCl_2$, $Sn(Ac)_4$, sodium oleate, diphenyl diselenide (98%), toluene, oleylamine, Se powder. All

chemicals were used directly without any purification. Cu-oleate was synthesized as reported.[29]

Synthesis of Wurtzite Cu₂SnSe₃ Nanocrystals (R1). In a typical synthesis, stoichiometric amounts of diphenyl diselenide and Cu-oleate (0.250 mmol) and 10 mL oleylamine were added in a three-neck flask and evacuated at 60 °C for 20 min. The solution was then heated to 240 °C under an argon atmosphere. At the same time, $Sn(Ac)_4$ (0.125 mmol) was mixed with 2 mL oleylamine in a vial, which was preheated to 70 °C on a hot plate. At 230 °C, the $Sn(Ac)_4$ solution was injected by syringe. After injection, the reaction was allowed to proceed for 30−60 min with continuous stirring. The reaction was terminated by removal of the heating mantle and allowed to cool to room temperature naturally. The product was washed using the same typical procedure (see Supporting Information for additional experimental details). The final nanocrystals were dispersed in toluene for further characterization.

Synthesis of Linear Cu₂SnSe₃ Heterostructure Nanocrystals (R2). Typically, stoichiometric amounts of diphenyl diselenide, CuCl (0.50 mmol), and $SnCl_2$ and 10 mL oleylamine were added in a three-neck flask and evacuated at 60 °C for 20 min. The solution was then heated to 310 °C under an argon atmosphere and allowed to proceed for 60 min with continuous stirring.

Synthesis of Cubic Cu₂SnSe₃ Nanocrystals (R3). Se powder (0.375 mmol) and 10 mL oleylamine were added in a three-neck flask and evacuated at 60 °C for 20 min. The solution was then heated to 300 °C under an argon atmosphere. At the same time, stoichiometric amounts of CuCl (0.250 mmol) and $SnCl_2$ were mixed with 1 mL oleylamine in a vial and heated up to 200 °C on a hot plate. At 300 °C, the metal chloride solution at 200 °C was injected by syringe. After injection, the reaction was allowed to proceed for 5 min with continuous stirring.

Synthesis of Cu₂SnSe₃ Tetrapod Nanocrystals (R4). In a typical process, CuCl (0.250 mmol) and 10 mL oleylamine were added in a three-neck flask and evacuated at 60 °C for 20 min. The solution was then heated to 290 °C under an argon atmosphere. At the same time, diphenyl diselenide (0.188 mmol) and $Sn(Ac)_4$ (0.125 mmol) were mixed with 2 mL oleylamine in a vial by ultrasonic at room temperature. At 290 °C, the diphenyl diselenide and $Sn(Ac)_4$ solution was injected by syringe. After injection, the reaction was allowed to proceed for 15 min with continuous stirring.

Characterization Methods. *Transmission and Scanning Electron Microscopy.* The morphology of Cu₂SnSe₃ nanocrystals was characterized by transmission electron microscopy (TEM) and angular dark-field scanning transmission electron microscopy (SEM) using a JEOL JEM-2011F, operating at an accelerating voltage of 200 kV.

X-ray Diffraction Analysis. X-ray diffractograms of drop-cast films of Cu₂SnSe₃ nanocrystals on a glass substrate were carried out on a PANalytical X'Pert MPD Pro using Cu Kα radiation with a 1D X'Celerator strip detector. Rietveld refinement was carried out using GSAS.[50]

Raman Spectroscopy. Raman spectroscopy measurements were performed on a Renishaw 1000 Raman spectrometer equipped with a charged-coupled device (CVD) detector and a HeNe 633 nm laser at room temperature. An objective lens (×20) was used to focus the lasers on the samples with 10% laser output power. The laser polarization angle was set at 0°. The spectra were collected in the range from 0 to 1000 cm⁻¹.

UV−vis-NIR Absorption Spectra. UV−vis-NIR spectroscopy of Cu₂SnSe₃ nanocrystals solution was carried out on a Cary 5000 UV−vis-NIR spectrophotometer.

■ RESULTS

Wurtzite Cu₂SnSe₃ Nanocrystals. For Cu₂SnSe₃, the wurtzite phase is metastable and can only be obtained in nanocrystal form and not in the bulk. The ternary crystals occur always from the insertion of Sn into preformed binary Cu−Se nanocrytals. Consequently, the optimum temperature to nucleate the binary chalcogenide, 240 °C, coupled with judicious selection of tin precursor (tin acetate) for

decomposition is needed (R1). As shown in Figures 1a and S1, the as-synthesized nanocrystals are well dispersed with an
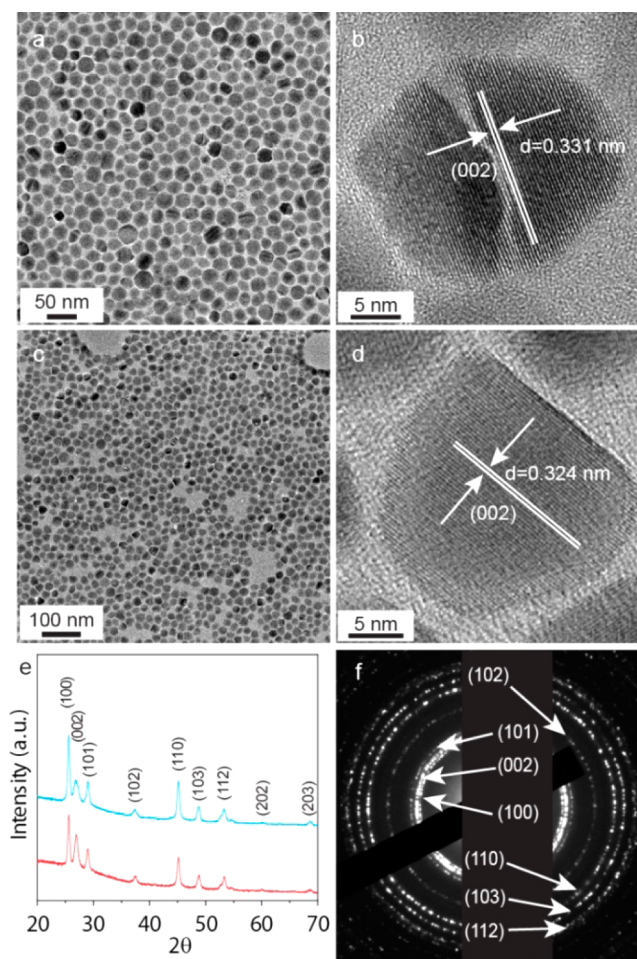

Figure 1. (a, c) Low-magnification TEM images of wurtzite nanocrystals. (b, d). HRTEM images of wurtzite nanocrystals. (e) XRD of wurtzite nanocrystals (blue, top: typical concentration (R1); red, bottom: halved concentration). (f) SAED pattern of typical wurtzite nanocrystals.

average diameter of 26.2 nm. A HRTEM image (Figure 1b) of an individual Cu₂SnSe₃ nanocrystal confirms the crystallinity with observed *d*-spacings (∼0.33 nm) corresponding to the (002) plane of wurtzite Cu₂SnSe₃. The shape of the nanocrystals also can be controlled by tuning the concentration. When the concentration of all reactants with respect to the olelylamine is halved, the resulting nanocrystals prefer to form pseudo round particles shown in Figure 1c,d rather than elongated nanocrystals. Clearly, the low chemical potential environment at low monomer concentrations limits the preference for growth along the *c*-axis.[2] The obtained particles are nearly monodisperse with an average diameter of 22.8 nm. Figure 1e shows the XRD patterns of as-synthesized nanocrystals samples both from typical (R1) and halved concentrations. The peaks match well with the simulated wurtzite structure.[46] The lattice parameter calculated from the experimental diffraction pattern is $a = b = 4.0139$ Å and $c = 6.6298$ Å, agreeing well with previous reports.[46,51,52] The selected-area electron diffraction (SAED) pattern (Figure 1f) can also be indexed with rings corresponding to the wurtzite Cu₂SnSe₃ phase.

Cubic Cu₂SnSe₃ Nanocrystals. Cubic phase nanocrystals were formed preferentially by switching to metal chloride salts with higher reaction temperatures of 300 °C while initially retaining diphenyl diselenide as the only chalcogen source (R3 using Ph_2Se_2 0.188 mmol). The XRD results, Figure 2a,
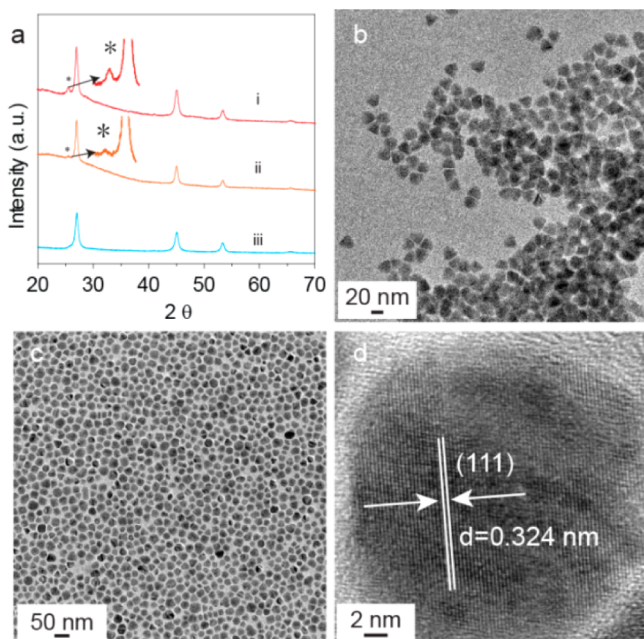

Figure 2. (a) XRD patterns of predominatly cubic nanocrystals with some wurtzite (i, (ii) and complete cubic (iii)). (b) Low-magnification TEM image of nanocrystals obtained at typical concentration (R3) with diphenyl diselenide. (c) Low-magnification TEM image of cubic structure nanocrystals. (d) HRTEM image of a single cubic nanocrystal.

indicate that the cubic phase dominates the product (curve (i)). Only the peak (100) with the highest intensity of all the peaks indexed to wurtzite phase was observed ($2\theta = 25.6°$ indexed with *), which confirms that the growth of wurtzite phase has been immensely suppressed. The resulting nanocrystals are nearly monodispersed with a triangular shape (Figure 2b). Reducing the concentration of all species (R3 using Ph_2Se_2 0.075 mmol, CuCl 0.100 mmol, and $SnCl_2$ 0.050 mmol) did lower the intensity of the wurtzite (100) peak (Figure 2a curve (ii)) while retaining nanocrystal formation (Figure S2). However, in our investigations, no matter what procedure was employed, pure cubic product is not obtained by using the reagent combination of metals chlorides and diphenyl diselenide. Switching the chalcogen source to selenium powder (R3) resulted in complete elimination of wurtzite Figure 2a (curve (iii)) with only cubic nanocrystals obtained. The XRD pattern can be indexed to bulk cubic Cu₂SnSe₃ (JCPDF 65-4145) crystals. The lattice parameter calculated from the experimental diffraction pattern is $a = 5.6919$ Å, consistent with values reported elsewhere.[51] Figures 2c and S1 show typical transmission and scanning electron microscopy images of the as-synthesized Cu₂SnSe₃ nanocrystals, which indicates that the nanocrystals are well dispersed with an average diameter of 28.0 nm. The SAED pattern (Figure S3) is also consistent with the cubic structure, indexed to (111), (220), and (311) planes, respectively. Figure 2d presents a HRTEM image of an individual NC. The lattice fringes show that the nanocrystal is a

single crystal with a d-spacing of 0.324 nm indexed to the (111) plane of cubic Cu₂SnSe₃.

Linear Heterostructure Cu₂SnSe₃ Nanocrystals. Clearly, modulating the temperature and choice of reactants has a significant effect on the morphology. Moreover, systematic variation of these parameters allows for interesting heterostructure formations. Combining diphenyl diselenide with the low-reactivity metal salts (R2) and allowing the temperature to ramp promotes the wurtzite nanocrystals to form first with termination in the cubic phase (once the conditions for this phase dominate). Figure 3a shows a
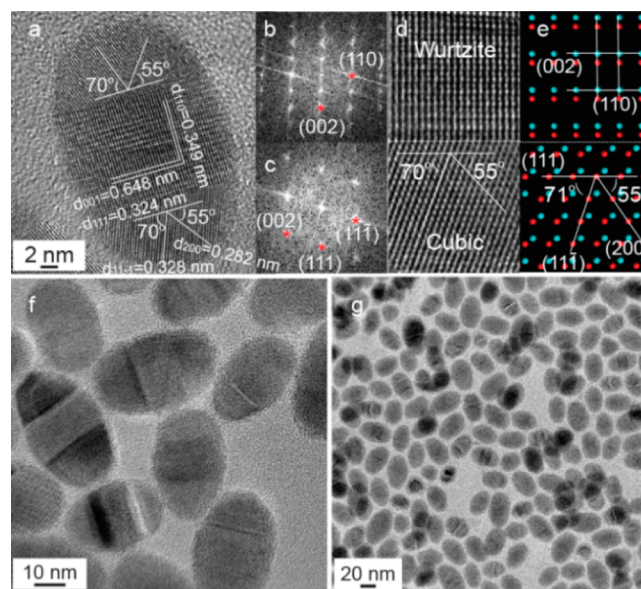

Figure 3. (a) HRTEM image of a Cu₂SnSe₃ linear heterostructured nanocrystal. (b−d) Magnified HRTEM image of the interface with their corresponding FFT. (e) Crystal model of the interface. (f, g) TEM images of linear heterostructured nanocrystals.

HRTEM image and the corresponding fast Fourier transform (FFT) images (Figure 3b,c) of a linear heterostructure nanocrytal to reveal the finer structural details. The nanocrytals compose three distinct but equal sized parts: the midbody is wurtzite structure, and the two end components are zinc-blende-derived (cubic) structures. For the core part, the observed d-spacings of 0.349 and 0.648 nm can be indexed to (110) and (001) planes of wurtzite. A HRTEM image and the corresponding crystal model (Figure 3d,e) show the interface of the two structures showing that the cubic structure epitaxially grows from wurtzite structure. The observed d-spacings (about 0.282, 0.324, and 0.328 nm) correspond to (200), (111), and (11-1) planes of the cubic phase. The observed angles also agree well with the theoretical values.[44] Figures 3f,g and S1 show the relative low-magnification TEM and SEM images, indicating that the synthesized nanocrystals have uniform rice-like shape and are well dispersed with an average long and short diameter of 36.8 and 24.6 nm, respectively.

The structure and composition of the as-synthesized Cu₂SnSe₃ linear heterostructure nanocrystals were further characterized by XRD and high-scanning transmission electron microscope energy dispersive spectrometer (STEM-EDS) elemental mapping and line scan. It should be noted that the peak at about 27° is asymmetric with a shoulder on the low

angle side. They can be refined to two peaks (26.8° and 27.1°), which can be indexed to the (002) plane of wurtzite structure and the (111) plane of cubic structure. Such an asymmetry implies that the amounts of the two phases are significant by XRD analysis. Rietveld refinement analysis was performed, and the result indicates that the synthesized sample is assuredly composed of the wurtzite and cubic phase, with a phase composition of 48.8% for the wurtzite structure. The SAED pattern can also distinguish the two planes: (002) of wurtzite and (111) of cubic, as shown in the inset of Figure 4a. Besides
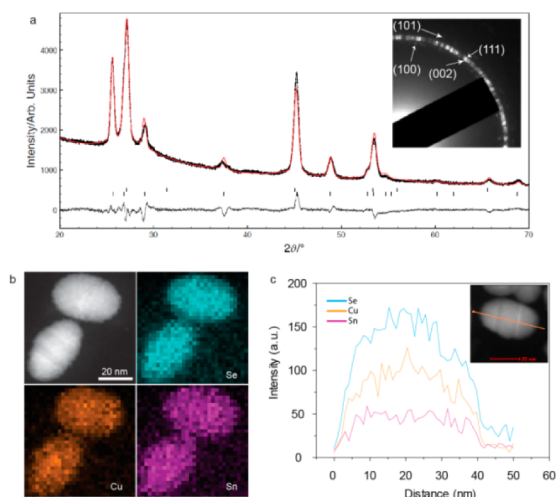

Figure 4. (a) XRD pattern and Rietveld fit of the obtained heterostructure nanocrstals (R_{wp}: 3.81% and R_p: 2.68%); the inset is the corresponding SAED pattern. (b) STEM image and STEM-EDS elemental mappings of Cu_2SnSe_3 heterostructures. (c) STEM-EDS line scan of one single Cu_2SnSe_3 heterostructure; the inset is the corresponding STEM image.

that, the contrast difference of the obtained product is clearly observed in TEM (Figure 3f) and bright-field TEM (Figure 4b,c) images. The contrast difference has been observed in some nanoheterostructure systems because of different mass-thickness and diffraction.[3,44] In order to clarify whether the contrast difference is from the composition variation, elemental mapping and line scan were recorded, Figure 4b,c, revealing the homogeneous distribution of the three elements with the Se/Cu/Sn ratio close to the expected 3:2:1.

Cu_2SnSe_3 Tetrapods. We recently demonstrated tetrapod formation in this system where nucleation occurs in the cubic phase with termination with four wurtzite arms from the four equivalent (111) faces.[46] In that study, we used nucleation and growth temperature as an effective method to tune phase preference with the higher preferring cubic with a subsequent drop allowing hexagonal to dominate. Here we show that reagent choice can also be utilized with a combination of diphenyl diselenide with the chloride salt of copper and the acetate salt of tin (R4) proving most effective with tetrapod nanocrystals dominating larger than 90% numerically. The large area TEM and SEM images (Figures 5a and S1) indicate that the as-synthesized tetrapods are nearly monodispersed with an average arm diameter of 16.9 nm and length of 15.8 nm. The XRD and SAED pattern (Figure S4) confirm the expected structure as shown in Figure 5b, with each tetrapod comprising the cubic core and wurtzite arms. The aspect ratio of the arms (~1) is very small in comparison to CdX tetrapods (X = S, Se, Te).[2,16,47] Increasing the concentration of selenium precursor
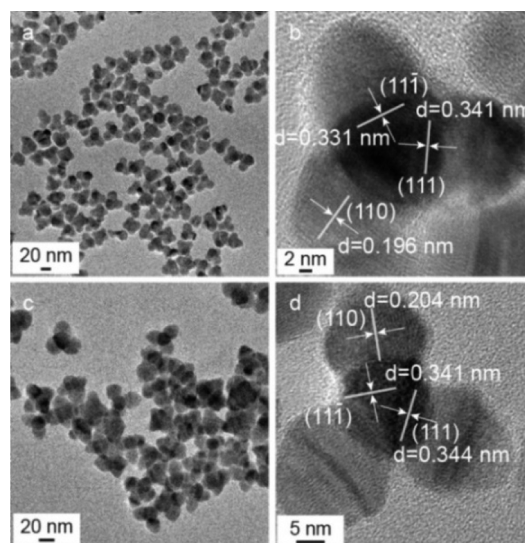

Figure 5. (a) Low-magnification TEM image of tetrapods. (b) HRTEM image of a single tetrapod. (c) Low-magnification TEM image of tetrapods at a higher diphenyl diselenide concentration. (d) HRTEM image of a single tetrapod.

(R4 Ph_2Se_2 0.375 mmol) results in an interesting shape change in the arms (Figure 5c,d). The arms elongated (length is 20.2 nm) but also noticeably widen at their central region most likely due to growth of the {110} facets. Clearly, when growth switches from the cubic phase to the hexagonal phase there is no preference for the (001) direction that favors anisotropic rod formation. Further work to get nanorods or tetrapods with longer arms is ongoing and will most likely only be obtained by the introduction of structure directing ligands that can passivate growth directions other than the (001). As yet, suitable ligands to affect this in compound copper selenides have proven difficult in comparison to the related sulfides where the dual functionality of thiols as a sulfur source and ligand proved effective.[18−20,43]

Raman spectra were further used to confirm the structure of the four products because binary compounds such as Cu_2Se have an XRD pattern that cannot be distinguished from that of Cu_2SnSe_3. Figure 6a shows the typical Raman spectra of the
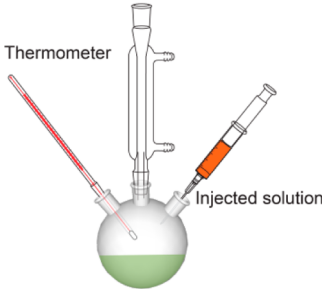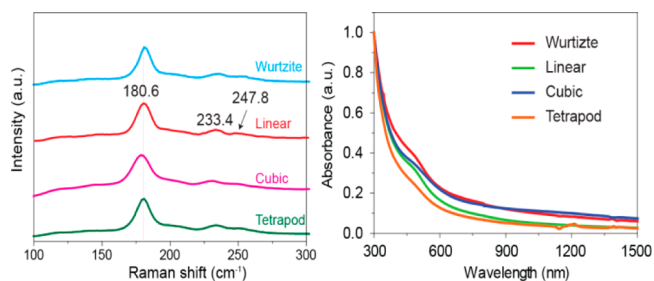

Figure 6. Raman and UV−vis−NIR absorption spectra of the as-synthesized products.

samples where three peaks are observed, at 180, 233, and 248 cm^{-1}, agreeing well with the reported modes.[53,54] The Raman shift for the strongest peak observed at ∼180 cm^{-1} can be assigned to the main mode of Cu_2SnSe_3, originating from the motion between the Se and Cu atoms as well as the Sn atom at rest. The absence of peaks around 260 cm^{-1}, corresponding to CuSe or Cu_2Se, and peaks around 150 and 110 cm^{-1},

7957

dx.doi.org/10.1021/ja501591n | J. Am. Chem. Soc. 2014, 136, 7954−7960

Table 1. Details of Reaction Condition for Four Types of Nanocrystals

Reaction	Phase	Precursors in flask	Injected precursors	Injection temperature	Growth temperature	Shape
R1	Wurtzite	Ph$_2$Se$_2$, Cu-Oleate	Sn(Ac)$_4$	230 °C	240 °C for 30min	
R2	Polytype 1	Ph$_2$Se$_2$, CuCl, SnCl$_2$	No injection	No injection	310 °C for 60 min	
R3	Cubic	Se	CuCl, SnCl$_2$	300 °C	300 °C for 5 min	
R4	Polytype 2	CuCl	Ph$_2$Se$_2$, Sn(Ac)$_4$	290 °C	280 °C for 15 min	

corresponding to SnSe or SnSe$_2$, confirmed the purity of the ternary Cu$_2$SnSe$_3$ phase without any additional binary compounds.[55,56] Energy dispersive X-ray spectroscopy was utilized to measure the composition of as-synthesized products. Measurement of more than five randomly selected areas gave average compositions as shown in Table S1. All the four samples are slightly selenium-rich (Se/(Cu + Sn) >1). The samples synthesized using diphenyl diselenide are slightly tin-rich (Cu/Sn < 2), and the cubic nanocrystals synthesized using Se powder are slightly tin-poor (Cu/Sn > 2), which probably is attributed to the different activities of Se precursors.

UV–vis–NIR absorption spectroscopy was used to investigate the optical properties of the four as-synthesized nanocrystals (R1−R4). All the nanocrystal types show significant absorption in the UV to visible spectral region with a shoulder peak at ~500 nm, consistent with previous reports.[51,52,54] The optical bandgap was estimated by using the method based on the relation of $(\alpha\hbar\nu)^2$ versus $\hbar\nu$ (where α is absorbance, $\hbar$ is Planck's constant, and ν is frequency). The results demonstrate effective optical bandgaps of ~1.54, ~1.36, ~1.34, and ~1.35 eV for wurtzite, linear, cubic, and tetrapod nanocrystals, respectively. It is unadvisable to reveal the influence of structure on the bandgaps because of their different sizes and compositions, but the bandgap of wurtzite structure is obviously larger than that of cubic structure, showing the same tendency with previous reports.[52]

DISCUSSION

The results collated in Table 1 show that phase control in colloidal syntheses of ternary chalcogenides is achievable although requires suitable balance of the control factors; in particular regent choice and respective nucleation and growth temperatures. While each of these factors can be tuned to direct the chemistry of the process, they cannot be considered in isolation. For example, we have previously shown that temperature can be effective to tune hexagonal or cubic growth with higher nucleation temperatures required for the cubic phase. Obtaining pure cubic nanocrytals, however, requires complete suppression of the wurtzite Cu$_2$SnSe$_3$ phase. This is where reagent choice becomes important. Diorgano dichalco-genides have been shown to be optimal low-temperature chalcogen sources for wurtzite nanocrystal syntheses as they are commonly more active than powder Se. This favors a faster reaction rate supporting the occurrence of dynamically stable products (wurtzite) at relatively low temperature. In contrast, at relatively high temperature the formation of thermodynamically stable products (cubic) will be dominant. In the presence of diphenyl diselenide and regardless of concentration or temperature, some wurtzite product was formed. Modifying

the reactivity of the cation precursors with the more active tin precursor (R3 using Sn(Ac)$_4$ instead of SnCl$_2$ at the same concentration) removed the wurtzite peak (Figure S5). However, impurities such as SnSe were observed, and large crystals were generated (Figure S5). This is likely to be due to Sn(Ac)$_4$ being too active to be compatible with CuCl and diphenyl diselenide to form a completely homogeneous Cu$_2$SnSe$_3$ phase. It has previously been shown that some anionic reactants favor thermodynamically stable products with Se powder with lower reactivity allowing formation of cubic crystals of selenides. This is confirmed in our observations where in the presence of Se powder the cubic Cu$_2$SnSe$_3$ phase is completely dominant regardless of when it is incorporated R3 (Figure S6).

Formation of the pure wurtzite phase can be achieved by maintaining the reaction temperature below the threshold for cubic crystal formation. This requires precursors that decompose at low temperature with diphenyl diselenide as Se precursor optimal. A precise temperature window is needed as temperature modulations were also seen to influence particle morphology and composition. At 220 °C, nearly round particles were obtained with the low content of Sn (Figure S7) most likely because the Cu ion exchange process was suppressed. Increasing the temperature to 255 °C resulted in the formation of polydisperse particles with some shape anisotropy (Figure S7). However, some nanocrytals with a small part of cubic phase were generated indicating the threshold for cubic phase nucleation was reached. Therefore, a moderate temperature (240 °C) was optimal to get pure wurtzite Cu$_2$SnSe$_3$ nanocrytals (R1).

Given that the wurtzite Cu$_2$SnSe$_3$ nanocrytals form at low temperature with cubic Cu$_2$SnSe$_3$ becoming favorable as the temperature increases, linear heterostructures were obtained by a facile approach where all precursors were present in the flask and the reaction is ramped up to 310 °C without any injection. As the temperature increases, the wurtzite phase nucleates with the growth of cubic phase epitaxially from wurtzite phase dominating at higher temperatures. Using precursors suitable for wurtzite (R1 using Cu-oleate, Ph$_2$Se$_2$, and Sn(Ac)$_4$ reacting at 280 °C) does generate some linear heterostructures, although the wurtzite nanocrystals are always dominant (Figure S8). Optimal control of the linear heterostructure was obtained by using the metal chlorides as the cation precursors with diphenyl diselenide as the anion and ramping to 310 °C with growth for 60 min (R2). The presence of diphenyl diselenide favors growth of hexagonal at low temperature regardless of the cation specie,s however at higher temperatures the metal chloride salts perturb the reaction more in favor of cubic growth in comparison to the acetate salts. This leads to

heterostructures with alternating and equal segments of both phases.

Our observations are that the windows for hexagonal (220–280 °C) and cubic growth (255–310 °C) overlap regardless of choice of precursors. Obtaining pure phases of either requires temperatures of <250 °C (hexagonal) with precursors that react at that temperature and >280 °C cubic where reactivity of precursors is balanced to allow ternary growth. For tetrapods the cubic crystals must nucleate first, however if we use selenium as the anionic precursor, no hexagonal phase occurs regardless of the temperature drop. Therefore, to satisfy this requirement, diphenyl diselenide with $Sn(Ac)_4$ was injected into the flask at high temperature −290 °C (R4) . The injection of a cold solution automatically drops down the temperature of the solution in the flask by about 10 °C just inside the wurtzite spectrum. Our observations from a range of experiments suggest that a rapid temperature perturbation will instigate a phase change and that in most cases this will happen if reaction conditions are suitable. Therefore, here nucleation in cubic is immediately followed by growth in the wurtzite crystal phase to terminate the 3D structure.

The conditions outlined in Table 1 for R1−R4 are optimal for the formation of monodisperse nanocrystals of each type. Variations from these protocols in terms of the reagent choice or whether injected or not will lead to nanocrystals that are generally polydisperse. In R1 and R2, where wurtzite nucleates first, the presence of copper and selenium precursors in the flask is optimal as the reaction proceeds with formation of the binary CuSe followed by gradual Sn insertion. However, for R3 and R4, with cubic nucleation, the cation and anion species must only combine at high temperatures.

CONCLUSION

In summary, a full investigation of Cu_2SnSe_3 phase formation in colloidal systems is outlined to show the key conditions to form uniform particles of each type wurtzite, cubic, linear heterostructures, and tetrapods. The rationale for the optimal reaction conditions for each is detailed allowing greater insights into the chemistry of this growth process. We have shown how the selection of precursors, how they are combined, and the temperatures at which they are nucleated and grown greatly affect the growth protocols and ultimately the phase and shape of the resultant particles. XRD, Raman, TEM, and energy dispersive X-ray spectroscopy confirmed the obtained products were highly pure Cu_2SnSe_3 phase in each case. These insights allow for a greater understanding of nucleation and growth in colloidal synthesis of compound semiconductor nanocrystals for a range of potential applications from electronics to photovoltaics. The facile synthesis strategy opens pathways for extension to other compositions of multielement copper chalcogenides where the cubic and hexagonal phases can be formed.

ASSOCIATED CONTENT

Ⓢ Supporting Information

Experimental details. More TEM, SEM images, XRD data, compositions of synthesized nanocrytals. This material is available free of charge via the Internet at http://pubs.acs.org.

AUTHOR INFORMATION

Corresponding Author

kevin.m.ryan@ul.ie

Notes

The authors declare no competing financial interest.

REFERENCES

(1) (a) Murray, C. B.; Norris, D. J.; Bawendi, M. G. *J. Am. Chem. Soc.* **1993**, *115*, 8706. (b) Kelly, D.; Singh, A.; Barrett, C. A.; O'Sullivan, C.; Coughlan, C.; Laffir, F. R.; O'Dwyer, C.; Ryan, K. M. *Nanoscale* **2011**, *3*, 4580.

(2) Peng, X. *Adv. Mater.* **2003**, *15*, 459.

(3) Mokari, T.; Sztrum, C. G.; Salant, A.; Rabani, E.; Banin, U. *Nat. Mater.* **2005**, *4*, 855.

(4) Li, H.; Zanella, M.; Genovese, A.; Povia, M.; Falqui, A.; Giannini, C.; Manna, L. *Nano Lett.* **2011**, *11*, 4964.

(5) Wang, J. J.; Hu, J. S.; Guo, Y. G.; Wan, L. J. *J. Mater. Chem.* **2011**, *21*, 17582.

(6) (a) Singh, S.; Singh, A.; Palaniappan, K.; Ryan, K. M. *Chem. Commun.* **2013**, *49*, 10293. (b) Singh, A.; Dickinson, C.; Ryan, K. M. *ACS Nano* **2012**, *6*, 3339. (c) Singh, A.; Gunning, R. D.; Ahmed, S.; Barrett, C. A.; English, N. J.; Garate, J.-A.; Ryan, K. M. *J. Mater. Chem.* **2012**, *22*, 1562.

(7) Talapin, D. V.; Lee, J.-S.; Kovalenko, M. V.; Shevchenko, E. V. *Chem. Rev.* **2009**, *110*, 389.

(8) Stavrinadis, A.; Rath, A. K.; de Arquer, F. P. G.; Diedenhofen, S. L.; Magén, C.; Martinez, L.; So, D.; Konstantatos, G. *Nat. Commun.* **2013**, *4*, 2981.

(9) Talapin, D. V.; Murray, C. B. *Science* **2005**, *310*, 86.

(10) Kovalenko, M. V.; Scheele, M.; Talapin, D. V. *Science* **2009**, *324*, 1417.

(11) Ibanez, M.; Zamani, R.; LaLonde, A.; Cadavid, D.; Li, W. H.; Shavel, A.; Arbiol, J.; Morante, J. R.; Gorsse, S.; Snyder, G. J.; Cabot, A. *J. Am. Chem. Soc.* **2012**, *134*, 4060.

(12) Ibanez, M.; Cadavid, D.; Anselmi-Tamburini, U.; Zamani, R.; Gorsse, S.; Li, W.; Lopez, A. M.; Morante, J. R.; Arbiol, J.; Cabot, A. *J. Mater. Chem. A* **2013**, *1*, 1421.

(13) Wang, J. J.; Lv, A. F.; Wang, Y. Q.; Cui, B.; Yan, H. J.; Hu, J. S.; Hu, W. P.; Guo, Y. G.; Wan, L. J. *Sci. Rep.* **2013**, *3*, 2613.

(14) Zhou, H.; Song, T.-B.; Hsu, W.-C.; Luo, S.; Ye, S.; Duan, H.-S.; Hsu, C.-J.; Yang, W.; Yang, Y. *J. Am. Chem. Soc.* **2013**, *135*, 15998.

(15) Milliron, D. J.; Hughes, S. M.; Cui, Y.; Manna, L.; Li, J. B.; Wang, L. W.; Alivisatos, A. P. *Nature* **2004**, *430*, 190.

(16) Manna, L.; Milliron, D. J.; Meisel, A.; Scher, E. C.; Alivisatos, A. P. *Nat. Mater.* **2003**, *2*, 382.

(17) Mainz, R.; Singh, A.; Levcenko, S.; Klaus, M.; Genzel, C.; Ryan, K.; Unold, T. *Nat. Commun.* **2014**, *5*, 3133.

(18) Singh, A.; Coughlan, C.; Laffir, F.; Ryan, K. M. *ACS Nano* **2012**, *6*, 6977.

(19) Singh, A.; Geaney, H.; Laffir, F.; Ryan, K. M. *J. Am. Chem. Soc.* **2012**, *134*, 2910.

(20) Wang, Y.-H. A.; Zhang, X.; Bao, N.; Lin, B.; Gupta, A. *J. Am. Chem. Soc.* **2011**, *133*, 11072.

(21) Tang, X.; Cheng, W.; Choo, E. S. G.; Xue, J. *Chem. Commun.* **2011**, *47*, 5217.

(22) Li, S.; Zhao, Z.; Liu, Q.; Huang, L.; Wang, G.; Pan, D.; Zhang, H.; He, X. *Inorg. Chem.* **2011**, *50*, 11958.

(23) Bao, N.; Qiu, X.; Wang, Y.-H. A.; Zhou, Z.; Lu, X.; Grimes, C. A.; Gupta, A. *Chem. Commun.* **2011**, *47*, 9441.

(24) Pan, D.; An, L.; Sun, Z.; Hou, W.; Yang, Y.; Yang, Z.; Lu, Y. *J. Am. Chem. Soc.* **2008**, *130*, 5620.

(25) Tang, J.; Hinds, S.; Kelley, S. O.; Sargent, E. H. *Chem. Mater.* **2008**, *20*, 6906.

(26) Connor, S. T.; Hsu, C.-M.; Weil, B. D.; Aloni, S.; Cui, Y. *J. Am. Chem. Soc.* **2009**, *131*, 4962.

(27) Guo, Q. J.; Hillhouse, H. W.; Agrawal, R. *J. Am. Chem. Soc.* **2009**, *131*, 11672.

(28) Guo, Q.; Ford, G. M.; Yang, W.-C.; Walker, B. C.; Stach, E. A.; Hillhouse, H. W.; Agrawal, R. *J. Am. Chem. Soc.* **2010**, *132*, 17384.

(29) (a) Wang, J. J.; Wang, Y. Q.; Cao, F. F.; Guo, Y. G.; Wan, L. J. *J. Am. Chem. Soc.* **2010**, *132*, 12218. (b) Zhang, Q.; Wang, J.-j.; Jiang, Z.; Guo, Y.-G.; Wan, L.-J.; Xie, Z.; Zheng, L. *J. Mater. Chem.* **2012**, *22*, 1765.

(30) Zhong, H.; Lo, S. S.; Mirkovic, T.; Li, Y.; Ding, Y.; Li, Y.; Scholes, G. D. *ACS Nano* **2010**, *4*, 5253.

(31) Wang, J. J.; Xue, D. J.; Guo, Y. G.; Hu, J. S.; Wan, L. J. *J. Am. Chem. Soc.* **2011**, *133*, 18558.

(32) Xie, Y.; Carbone, L.; Nobile, C.; Grillo, V.; D'Agostino, S.; Della Sala, F.; Giannini, C.; Altamura, D.; Oelsner, C.; Kryschi, C.; Cozzoli, P. D. *ACS Nano* **2013**, *7*, 7352.

(33) Xie, Y.; Riedinger, A.; Prato, M.; Casu, A.; Genovese, A.; Guardia, P.; Sottini, S.; Sangregorio, C.; Miszta, K.; Ghosh, S.; Pellegrino, T.; Manna, L. *J. Am. Chem. Soc.* **2013**, *135*, 17630.

(34) Fan, F.-J.; Wu, L.; Yu, S.-H. *Energy Environ. Sci.* **2014**, *7*, 190.

(35) Singh, A.; Singh, S.; Levcenko, S.; Unold, T.; Laffir, F.; Ryan, K. M. *Angew. Chem., Int. Ed.* **2013**, *52*, 9120.

(36) Koo, B.; Patel, R. N.; Korgel, B. A. *J. Am. Chem. Soc.* **2009**, *131*, 3134.

(37) Koo, B.; Patel, R. N.; Korgel, B. A. *Chem. Mater.* **2009**, *21*, 1962.

(38) Norako, M. E.; Brutchey, R. L. *Chem. Mater.* **2010**, *22*, 1613.

(39) Lu, X.; Zhuang, Z.; Peng, Q.; Li, Y. *CrystEngComm.* **2011**, *13*, 4039.

(40) Jiang, C. Y.; Lee, J. S.; Talapin, D. V. *J. Am. Chem. Soc.* **2012**, *134*, 5010.

(41) Liu, Y.; Yao, D.; Shen, L.; Zhang, H.; Zhang, X. D.; Yang, B. *J. Am. Chem. Soc.* **2012**, *134*, 7207.

(42) Wang, J. J.; Hu, J. S.; Guo, Y. G.; Wan, L. J. *NPG Asia Mater.* **2012**, *4*, e2.

(43) Coughlan, C.; Singh, A.; Ryan, K. M. *Chem. Mater.* **2013**, *25*, 653.

(44) Fan, F.-J.; Wu, L.; Gong, M.; Chen, S. Y.; Liu, G. Y.; Yao, H.-B.; Liang, H.-W.; Wang, Y.-X.; Yu, S.-H. *Sci. Rep.* **2012**, *2*, 952.

(45) Ibáñez, M.; Zamani, R.; Li, W.; Cadavid, D.; Gorsse, S.; Katcho, N. A.; Shavel, A.; López, A. M.; Morante, J. R.; Arbiol, J.; Cabot, A. *Chem. Mater.* **2012**, *24*, 4615.

(46) Wang, J.; Singh, A.; Liu, P.; Singh, S.; Coughlan, C.; Guo, Y.; Ryan, K. M. *J. Am. Chem. Soc.* **2013**, *135*, 7835.

(47) Li, H.; Kanaras, A. G.; Manna, L. *Acc. Chem. Res.* **2013**, *46*, 1387.

(48) Buonsanti, R.; Carlino, E.; Giannini, C.; Altamura, D.; De Marco, L.; Giannuzzi, R.; Manca, M.; Gigli, G.; Cozzoli, P. D. *J. Am. Chem. Soc.* **2011**, *133*, 19216.

(49) Zamani, R. R.; Ibáñez, M.; Luysberg, M.; García-Castelló, N.; Houben, L.; Prades, J. D.; Grillo, V.; Dunin-Borkowski, R. E.; Morante, J. R.; Cabot, A.; Arbiol, J. *ACS Nano* **2014**, *8*, 2290.

(50) Larson, A.; Von Dreele, R. General Structure Analysis System (GSAS). *Report LAUR 86-748*; Los Alamos National Laboratory: Los Alamos, NM2004.

(51) Li, S.; Pan, D. *J. Cryst. Growth.* **2012**, *358*, 38.

(52) Norako, M. E.; Greaney, M. J.; Brutchey, R. L. *J. Am. Chem. Soc.* **2012**, *134*, 23.

(53) Marcano, G.; Rincon, C.; Lopez, S. A.; Sanchez Perez, G.; Herrera-Perez, J. L.; Mendoza-Alvarez, J. G.; Rodriguez, P. *Solid State Commun.* **2011**, *151*, 84.

(54) Ahmadi, M.; Pramana, S. S.; Batabyal, S. K.; Boothroyd, C.; Mhaisalkar, S. G.; Lam, Y. M. *Inorg. Chem.* **2013**, *52*, 1722.

(55) Tanaka, T.; Sueishi, T.; Saito, K.; Guo, Q.; Nishio, M.; Yu, K. M.; Walukiewicz, W. *J. Appl. Phys.* **2012**, *111*, 053522.

(56) Ishii, M.; Shibata, K.; Nozaki, H. *J. Solid. State. Chem.* **1993**, *105*, 504.

7960

dx.doi.org/10.1021/ja501591n | *J. Am. Chem. Soc.* 2014, 136, 7954–7960